doi: 10.4149/gpb_2025022

Hypoxia-conditioned cardiomyocyte-derived exosomes attenuate myocardial injury *via* ANP-mediated M2 macrophage polarization

Mingye Wang[1,*], Chi Zhao[2,*], Tongtong Li[1,3,*], Tao Song[4], Yuanyuan Hao[4], Wenwen Cui[4], Min Guan[5], Yunlong Hou[1,2,6,7] and Yang Li[5]

[1] *College of Integrated Traditional Chinese and Western Medicine, Hebei University of Chinese Medicine, Shijiazhuang, Hebei, China*
[2] *Hebei Medical University, Shijiazhuang, Hebei, China*
[3] *Affiliated Yiling Hospital of Hebei Medical University, Shijiazhuang, Hebei, China*
[4] *Shijiazhuang Yiling Pharmaceutical Co., Ltd, New Drug Evaluation Center, Shijiazhuang, Hebei, China*
[5] *Department of Cardiology, The Fourth Affiliated Hospital of Harbin Medical University, Nangang District, Harbin, Heilongjiang, China*
[6] *State Key Laboratory for Innovation and Transformation of Luobing Theory, Shijiazhuang, Hebei, China*
[7] *Shijiazhuang New Drug Technology Innovation Center of Compound Traditional Chinese Medicine, Shijiazhuang, Hebei, China*

Abstract. Exosomes derived from various cells have been demonstrated to contribute to cardiac repair by regulating macrophage polarization in myocardial infarction. However, how exosomes secreted from cardiomyocytes under hypoxia-ischemia (Hypo-Exo) regulate macrophage polarization in the local tissues is elusive. This study aimed to determine the underlying mechanisms by which Hypo-Exo polarized M2 macrophages. Hypo-Exo was harvested from the supernatant of oxygen glucose deprivation (OGD)-conditioned H9c2, identified using transmission electron microscopy, nanoparticle tracking analysis, and Western blot, and then applied to RAW264.7 and C57BL/6N mice. Echocardiography, TTC, H&E, Masson, and immunofluorescence staining were used to evaluate the therapeutic effects of Hypo-Exo in the myocardial infarction injury (MI) mouse model. The effects of Hypo-Exo on RAW264.7 were examined by RT-qPCR. Hypo-Exo labeled with PKH26 could be engulfed by RAW264.7 cells and promote M2 macrophage polarization. Hypo-Exo inhibited atrial natriuretic peptide (ANP) mRNA expression in RAW264.7 cells, and three cargo miRNAs of Hypo-Exo were upregulated to degrade the ANP expression. Instead of downregulating ANP, OGD supernatant upregulated ANP expression to activate M1 macrophages. Our study demonstrated a novel mechanism that Hypo-Exo carried with miRNAs as a communicator to degrade the expression level of ANP mRNA in macrophages by which Hypo-Exo polarized M2 macrophages to improve recovery from MI in mice.

Key words: Hypo-Exo — Macrophages — ANP — Myocardial infarction — Inflammatory

* These authors contributed equally to this paper.
Electronic supplementary material. The online version of this article (doi: 10.4149/gpb_2025022) contains Supplementary material.
Correspondence to: Yunlong Hou, College of Integrated Traditional Chinese and Western Medicine, Hebei University of Chinese Medicine, Shijiazhuang 050091, Hebei, China
E-mail: houyunlonghrb@hotmail.com
Yang Li, Department of Cardiology, The Fourth Affiliated Hospital of Harbin Medical University, No.37, Yiyuan Street, Nangang District, Harbin 150000, Heilongjiang, China
E-mail: doctoryangli@hrbmu.edu.cn

Abbreviations: ANP, atrial natriuretic peptide; BSA, bovine serum albumin; DAPI, 4′,6-diamidino-2-phenylindole; FBS, fetal bovine serum; HF, heart failure; Hypo-Exo, exosomes secreted from cardiomyocytes under hypoxia-ischemia; IL-1β, interleukin-1β; iNOS, inducible nitric oxide synthase; LAD, left anterior descending; MSCs, mesenchymal stem cells; NTA, nanoparticle tracking analysis; OGD, oxygen glucose deprivation; PBS, phosphate-buffered saline; TBST, Tris buffered saline containing 0.1% Tween 20; TEM, transmission electron microscopy; TNF-α, tumor necrosis factor-α.

Introduction

Myocardial infarction, a life-threatening emergency, is caused by the interruption of blood flow to the heart muscle, leading to irreversible necrosis in myocardial tissue and a secondary process of tissue repair (Anderson and Morrow 2017). Although the mortality of coronary heart disease has gradually declined over the past decades (Nichols et al. 2014), with approximately 550,000 new cases and 200,000 recurrent episodes of acute myocardial infarction appearing annually, myocardial infarction retains a significant influence on global health (Anderson and Morrow 2017).

According to previous studies (Mezzaroma et al. 2011), the recruitment of immune cells and secretion of pro-inflammatory cytokines occur in the early phases of myocardial infarction to eliminate the apoptotic or necrotic cells and participate in post-injury repair. Among leucocytes, monocytes and macrophages play pivotal roles in maintaining cardiac homeostasis and modulating inflammatory processes (Moskalik et al. 2022). Due to the diverse phenotypes, macrophages are generally divided into M1 and M2 subtypes (Murray et al. 2014; Sica et al. 2015; Shapouri-Moghaddam et al. 2018). M1 macrophages are pro-inflammatory and secrete pro-inflammatory cytokines such as interleukin-1β (IL-1β), IL-6, IL-12, IL-23, tumor necrosis factor-α (TNF-α), and inducible nitric oxide synthase (iNOS), exerting phagocytotic effects and inflammatory cascades. Instead, M2 macrophages are thought to be anti-inflammatory and secrete higher IL-10 and TGF-β, reducing inflammatory reactions and promoting tissue repair (Jung et al. 2017; Ma et al. 2018; Peet et al. 2020). The numbers of monocytes and macrophages in the heart expand rapidly in the days after myocardial infarction (Lee et al. 2012; Jung et al. 2013). These initial infiltrating cells demonstrate a pro-inflammatory phenotype, which is dominated by inflammatory Ly-6c^{high} M1 macrophages responsible for clearing cell debris from the infarcted region. Then Ly-6c^{low} M2 macrophages become dominant in the heart tissue to inhibit the inflammatory reaction and preserve cardiac functionality. Thus, due to the high plasticity and diverse phenotypes, macrophages have a profound impact on the pathophysiological process of myocardial infarction. Therefore, the plasticity of macrophages could be utilized to improve post-myocardial infarction injury, and a thorough understanding of macrophage polarization could be promising for figuring out a therapeutic target and a novel therapeutic strategy.

Recently, exosomes, a king of membrane vesicles secreted by most cell types, have been recognized as new candidates with essential roles in intercellular communication (Sahoo and Losordo 2014; Benecke et al. 2021). Recent studies indicated that exosomes stemmed from mesenchymal stem cells (MSCs) attenuate myocardial I/R injury in mice, and the exosomes secreted by hypoxia-conditioned MSCs facilitate ischemic cardiac repair (Zhu et al. 2018) by regulating the miRNA expression to modify the macrophage polarization towards the M2 subtype *in vivo* and *in vitro* (Vandergriff et al. 2018; Zhao et al. 2019; Gao et al. 2020; Xiong et al. 2021; Zhang et al. 2022). Moreover, as a critical intercellular communicator, cardiomyocyte-derived exosomes could also regulate the macrophage polarization towards M2 macrophages to reduce the apoptosis of cardiomyocytes. Emerging evidence suggests that the exosomes might have potential as a therapeutic regime in myocardial I/R injury. However, the underlying mechanism of exosomes in macrophage polarization is still elusive.

The natriuretic peptide (NP) system in heart tissue is a family of hormones with pleiotropic effects, including atrial NP (ANP), B-type NP (BNP), C-type NP (CNP), Dendroaspis NP, and Urodilatin. In general, NPs represent a kind of intrinsic antihypertensive hormones and play central roles in the regulation of heart failure (HF), especially for both BNP and N-terminal proBNP as a biomarker to make the diagnosis and predict the prognosis in patients with HF (Fu et al. 2018). In recent years, mounting evidence indicates that NPs reduce infarcted areas and prevent adverse post-infarction remodeling of the heart. Moreover, the cardioprotective effects of NPs have been proven to be related to the anti-apoptotic and anti-inflammatory effects (Krylatov et al. 2021), and ANP attenuates myocardial injuries and improves left ventricular function in the rat model of myocardial ischemia-reperfusion injury (Fujii et al. 2012). Regarding the immunomodulatory effects of ANP (Kiemer and Vollmar 2001), both endogenous ANP and its receptors express in the macrophages, suggesting that ANP functions as an autocrine regulator and plays a vital role in regulating the production of inflammatory mediators in macrophages

(Vollmar and Schulz 1995; Kiemer and Vollmar 2001). However, whether the anti-inflammatory effects of ANP underpin myocardial protection and the underlying mechanism of immunoregulating activities have been elusive.

In this study, the culture media was collected from H9c2 cells in an ischemia-reperfusion model *in vitro* to activate the RAW264.7 cells. Exosomes were isolated from the culture media to validate the activation of RAW264.7 cells. Furthermore, exosomes derived from the supernatant of oxygen glucose deprivation-conditioned H9c2 (Hypo-Exo) were applied by intramyocardial injection around the infarcted areas in the mice myocardial infarction model to evaluate the potential of exosomes in the treatment of myocardial infarction. To further exploit the underlying mechanism of exosomes in macrophage polarization, we evaluated the expression level of the Hypo-Exo carried with miRNAs.

Materials and Methods

Cell culture and establishment of oxygen glucose deprivation (OGD) model in vitro

The mouse monocytic cell line RAW264.7 was purchased from the cell bank of the Chinese Academy of Sciences (Shanghai, China). H9c2 cells were obtained from Procell Life Science &Technology Co., Ltd (Wuhan, China). RAW264.7 and H9c2 cells were cultured in Dulbecco's Modified Eagle's Medium (DMEM; Gibco, USA) with 10% Fetal bovine serum (FBS) and 1% penicillin/streptomycin at 37°C and 5% CO_2.

When H9c2 cells reached approximately 80–90% confluence, H9c2 cells were inoculated into 100×20 mm style dishes. The next day, the culture medium was removed, and the cells were washed thrice with phosphate-buffered saline (PBS) and then cultured for 24 h with 10 ml glucose-free DMEM medium at 37°C in an anaerobic chamber, which was cultured with 94% N_2, 5% CO_2 and 1% O_2. And then, the supernatant was collected and set aside for subsequent experiments.

The treatment of RAW264.7 cells by supernatant of OGD

When cells reached approximately 80% confluence, RAW264.7 cells were seeded in 6-well plates at a density of 3×10^5 cells/well and incubated for 24 h. Then, the supernatant of OGD was diluted 10-fold with the complete DMEM medium (complete DMEM medium = 89% DMEM + 10% FBS + 1% penicillin/streptomycin) and added to the cells after removing the original supernatant and washing the cells with PBS. Each well received 2 ml of the diluted OGD supernatant.

Exosomes isolation

Exosomes were purified from the supernatant of H9c2 cells cultured under oxygen and glucose deprivation conditions (Hypo-Exo) by ultracentrifugation (Thery et al. 2006). Briefly, the supernatant of OGD was collected and centrifuged at 300×*g* for 10 min at 4°C. The supernatant was transferred to a new 15 ml centrifuge tube and centrifuged at 2000×*g* for 10 min at 4°C to exclude cellular debris and cells. Next, the supernatant was transferred to polyallomer tubes and centrifuged at 10,000×*g* for 30 min at 4°C. Then, the supernatant was collected into new polyallomer tubes and centrifuged at 100,000×*g* for 70 min at 4°C. The supernatant was removed as much as possible, and the pellet was resuspended with 1 ml PBS, then centrifuged at 100,000×*g* for 70 min at 4°C. Finally, exosomes were resuspended in PBS and stored at −80°C until further after quantification using a BCA Protein Assay Kit (Cot.PQ0012; Multi Sciences, China).

Transmission electron microscopy (TEM) and Nanoparticle tracking analysis (NTA)

TEM visualized the morphology of Hypo-Exo. Briefly, 20 μl of exosomes were loaded on carbon-coated copper electron microscopy grids for 2 min. Then, the samples were negatively labeled with a phosphotungstic acid solution for 5 min. The grids were washed thrice with PBS and maintained under semi-dry conditions. Images were obtained with a Hitachi HT-7700 TEM at 80 kV.

The concentration and particle size of Hypo-Exo were analyzed using nanoparticle tracking analysis with ZetaView-PMX120-Z (Particle Metrix, Meerbusch, Germany) and corresponding software ZetaView (version 8.05.14 SP7). In brief, the exosome samples were appropriately diluted using 1×PBS buffer to measure the concentration and particle size. NTA measurement was recorded and analyzed at 11 positions, and the ZetaView software was calibrated using 110 nm polystyrene particles.

Western blot analysis

Western blotting was used to identify the exosome markers TSG101 (ab125011; Abcam, USA) and CD63 (ab217345; Abcam). Briefly, the samples were mixed with loading buffer, heated at 95°C for 5 min, separated by SDS-PAGE, and transferred onto polyvinylidene fluoride (PVDF) membranes. The membranes were blocked with rapid blocking buffer (SEVER, Wuhan, China) for 30 min and then incubated with TSG101 (1:1000) and CD63 (1:1000) at 4°C overnight. The membranes were washed thrice with tris buffered saline containing 0.1% tween 20 (TBST) and incubated with a secondary antibody (1:5000) for one hour at room temperature. Signals were detected by the Odyssey

imaging system and quantified by image analysis software (LI-COR, Biosciences, USA).

Uptake of Hypo-Exo by RAW264.7 cells

Hypo-Exo was labeled with the red fluorescent dye PKH26 (BB-441125; Bestbio, China), and minor modifications were made according to the manufacturer's instructions. 2 μl PKH26 and 50 μl exosomes suspension were mixed gently and incubated at 37°C for 10 min. The labeling reaction was stopped by adding 50 μl PBS containing 0.5% BSA. The RAW264.7 cells were inoculated in 24-well plates at 1×10^5 cells/well density. After cell attachment, the PKH26-labelled exosomes were added and cocultured with RAW264.7 cells for 4 h. Then, the medium was removed and fixed with 4% paraformaldehyde solution for 20 min at room temperature and washed thrice with PBS. Nuclei were stained with 4',6-diamidino-2-phenylindole (DAPI) for 10 min. Finally, the uptake of exosomes by macrophages was observed by a fluorescence microscope.

Animals and ethical approval

A total of 36 C57BL/6N mice (male, 22–25 g) were obtained from the Vital River Laboratory Animal Technology Co. Ltd (NO. SCXK (Jing) 2021-0006, Beijing, China). The mice were randomly divided into three groups: Sham group (Sham, $n = 12$); myocardial infarction injury model group (MI, $n = 12$); acute myocardial infarction injury + Hypo-Exo (MI-Hypo-Exo, $n = 12$). A detailed breakdown of animal allocation and sample sizes for each analysis is provided in Supplementary Material, Table S1. The mice were housed in the standard laboratory conditions that contained a normal 12-h cycle of day and night and a temperature-controlled environment (20–26°C) in cages. The standard maintenance diet for mice and pure water were available *ad libitum*.

All experiments were carried out according to the "Guiding Opinions on Treating Laboratory animals" (Ministry of Science and Technology). All animal experimental procedures and welfare followed the Ethics Review Committee for Animal Experimentation of New Drug Evaluation Center of Hebei Yiling Medical Research Institute (protocol number: N20221122).

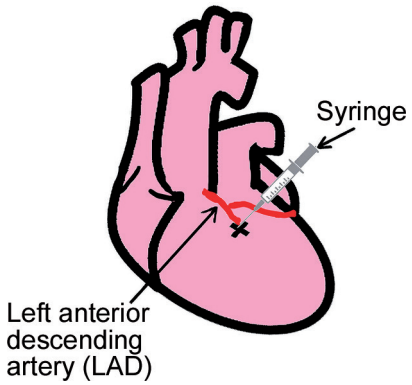

Figure 1. Schematic illustrations of the Hypo-Exo application by direct intramyocardial injection. The simple red lines represent the left coronary artery, the surgical ligation site. After ligation, the heart would gradually turn white, indicating successful modeling. Then a 30 G needle was introduced into the base of the heart above the area of the infarct border zone with 40 μl Hypo-Exo solution (The infarct border zone in MI models was to use the percentage of the LV wall volume that is affected by the infarction).

Myocardial infarction animal model creation, exosomes injection, and echocardiography

The myocardial infarction animal model was established by left anterior descending coronary artery (LAD) ligation (Virag and Lust 2011; Malliaras et al. 2013). Mice were anesthetized by a single intraperitoneal (i.p) injection of 2% pentobarbital (40 mg/kg) supplemented with an analgesic agent, butorphanol (0.25 mg/kg i.p.), and fur was removed from the skin of the left chest side. The mice were fixed to a plate and performed tracheal cannula to administer constant positive pressure ventilation. A left thoracotomy was conducted in the fourth intercostal space, and the left anterior descending artery was ligated with 8-0 polyethylene suture. The visual inspection or changes in electrocardiography was used to verify ischemia. The Sham group underwent the same procedure above, excluding the LAD ligation. Mice of the M-Hypo-Exo group were then subjected to intramyocardial injections with a 30G needle into the heart above the area of the infarct border zone with 40 μl Hypo-Exo solution (Fig. 1). The thoracic cavity was closed with 6-0 suture when the myocardial manipulations were completed, and the mice breathing rhythmically and shallowly were extubated. After surgery, mice were kept on a warming pad until they recovered their mobility. Then, they were returned to their cages and housed under standard laboratory conditions. At 72 h post-surgery, mice in the Sham, MI, and MI-Hypo-Exo groups were anesthetized with isoflurane (2.5% isoflurane in 0.8% oxygen) delivered by an anesthetic machine with a custom-made face mask ($n = 6$ each group). Their cardiac function was assessed by echocardiography using a Vevo 770TM Imaging System (VISUALSONICS). After completing cardiac ultrasound imaging, the hearts of mice were extracted, fixed, embedded in paraffin blocks, and sectioned into 4 μm-thick slices for subsequent tissue staining experiments.

Infarct size determination

The infarct size of hearts was tested by 2,3,5-triphenyl tetrazolium chloride (TTC). After 72 h surgery, mice of Sham,

MI, and MI-Hypo-Exo groups were euthanized with an overdose of pentobarbital sodium (120 mg/kg i.v. bolus), and the hearts of mice were harvested (n = 6 each group). The hearts were rapidly taken and frozen at −20°C for about 20–30 min, and then serially cross-sectioned in 1 mm thick sections. The slices were incubated in TTC with a concentration of 2% for 20 min at 37°C. Then slices were fixed in 10% paraformaldehyde for 24 h, and photographed. Image-Pro Plus 6.0 was used for Image analysis. Infarct area was quantified as INF/AAR×100%.

Histopathological analysis

The slices of heart tissues were dewaxed by using a dewaxing machine. Then sections were stained with Mayer's hematoxylin solution and eosin. Slices were dehydrated with ethanol and sealed with neutral gum. Finally, the morphological changes of heart tissues were observed under a microscope.

Masson staining

The Masson's Trichrome Stain Kit (G1340, Solarbio) was used to evaluate the degree of fibrosis in cardiac tissues according to the manufacturer's protocol. The results of the quantitative were analyzed with ImageJ software.

Double immunofluorescence staining

The slices of heart tissues were deparaffinized, subjected to antigen retrieval, and blocked with immunofluorescence staining blocking buffer (P0102; Beyotime, Shanghai, China) for one hour. Next, the slices were incubated overnight at 4°C with a mixture of two primary antibodies: anti-CD68 (1:500, ab125212) and anti-iNOS (1:250, SC-7271). The following day, the slices were washed three times with PBS and incubated for one hour at 37°C in the dark with a mixture of two secondary antibodies: Alexa Fluor 488-labeled donkey anti-rabbit IgG antibody (A0423, Beyotime) and Alexa Fluor 555-labeled donkey anti-mouse IgG antibody (A0460, Beyotime). After another three washes with PBS, the slices were mounted with a medium containing DAPI. The images were acquired using a confocal microscope (LSM710, Zeiss, Germany) and analyzed with ImageJ software.

Evaluation of ANP secretion by ELISA

The amount of ANP released in the supernatant of OGD was measured by ELISA, with the Rat ANP ELISA Kit (ZC-37379; ZCi Bio, Shanghai, China), following the manufacturer's instructions.

The treatment of RAW264.7 cells by Hypo-Exo

Briefly, RAW264.7 cells were inoculated into 6-well plates at a density of 3×10^5 cells/well. The next day, the cells were treated with Hypo-Exo for 24 h and then collected to detect relevant indicators.

RT-qPCR

The expression levels of *CD68*, *iNOS*, *IL-6*, *TNF-α*, *CD206*, *Arg1*, *ANP*, *NPR-A*, *miR-425*, *miR-155*, *miR-1-3p*, and *GAPDH* were detected by RT-qPCR (Primer sequences are shown in Table 1). In brief, total RNA was extracted from cells using the Eastep® Super total RNA extraction kit (Promega, Shanghai, China). The purity and concentration of RNA were determined with a Thermo Scientific NanoDrop One, and then the samples were stored at −80°C. The reverse transcription was performed using the GoScript™ Reverse Transcription System (Promega, Shanghai, China), and

Table 1. Primer sequences were used for RT-qPCR in this study

Primer (mouse)	Forward	Reverse
CD68	5'-GGGGCTCTTGGGAACTACAC-3'	5'-GTACCGTCACAACCTCCCTG-3'
iNOS	5'-AGACCTCAACAGAGCCCTCA-3'	5'-GCAGCCTCTTGTCTTTGACC-3'
IL-6	5'-CAACGATGATGCACTTGCAGA-3'	5'-TGACTCCAGCTTATCTCTTGGT-3'
TNF-α	5'-GATCGGTCCCCAAAGGGATG-3'	5'-TTGCTACGACGTGGGCTATC-3'
CD206	5'-GCACTGGGTTGCATTGGTTT-3'	5'-CCTGAGTGGCTTACGTGGTT-3'
Arg1	5'-TGTGAAGAACCCACGGTCTG-3'	5'-TACGTCTCGCAAGCCAATGT-3'
ANP	5'-CTGCTTCGGGGGTAGGATTG-3'	5'-GCTCAAGCAGAATCGACTGC-3'
NPR-A	5'-GCCTGCAACCAAGACCACTT-3'	5'-CGGTTCACACGTTTCACAGC-3'
miR425	5'-AATGACACGATCACTCCC-3'	5'-CAGTGCGTGTCGTGGAGT-3'
miR155	5'-GGCCTTAATGCTAATTGTGATA-3'	5'-CAGTGCGTGTCGTGGAGT-3'
miR-1-3p	5'-GGCTGGAATGTAAAGAAGTA-3'	5'-CAGTGCGTGTCGTGGAGT-3'
GAPDH	5'-GGTGAAGGTCGGTGTGAACG-3'	5'-CTCGCTCCTGGAAGATGGTG-3'

RT-qPCR reactions were performed in duplicates using the GoTaq® qPCR Master Mix (Promega, Shanghai, China) according to the manufacturer's protocol. Relative gene expression was calculated by using the $2^{-\Delta\Delta Ct}$ method, with GAPDH being used for normalization.

Statistical analysis

The results were presented as mean ± SD. Statistical analyses were performed using GraphPad Prism 9.0 software and SPSS 22.0. The data of normality and variance homogeneity were assessed by Levene's test. Statistical significance was calculated using an unpaired Student's *t*-test when two groups were compared or one-way ANOVA with Tukey's multiple comparison test to determine differences among multiple groups. Differences were considered statistically significant when the *p*-value was less than 0.05.

Results

Characterization of exosomes derived from cardiomyocytes

Hypo-Exo was harvested from the supernatant of hypoxia-conditioned H9c2, and the specific markers of exosomes (TSG101, CD63) were detected by Western blot (Fig. 2A). TEM visualized the morphology of Hypo-Exo and showed the presence of round or cup-shaped (Fig. 2B). NTA analyzed the vesicle size distribution within the 50–160 nm range (Fig. 2C).

Hypo-Exo could be engulfed by macrophages in vitro

The Hypo-Exo was labeled with PKH26 (red fluorescence) and cocultured with RAW264.7 cells for four hours. As shown in Figure 2D, the labeled Hypo-Exo could be observed in the macrophages of the PKH+Hypo-Exo group. The result showed that Hypo-Exo could be engulfed by RAW264.7 cells *in vitro*.

Hypo-Exo could alleviate heart tissue damage in vivo

Mice were subjected to echocardiography analysis 72 h after surgery or treatment (Fig. 3A). As shown in Figures 3B and C, representative results of the MI group showed that fractional shortening and ejection fraction in the MI group were significantly reduced compared with the sham group. However, fractional shortening and ejection fraction in the MI+Hypo-Exo group were significantly increased compared with the MI group.

As shown in Figure 3D, TTC staining reflected left anterior descending coronary artery (LAD) ligation that led to

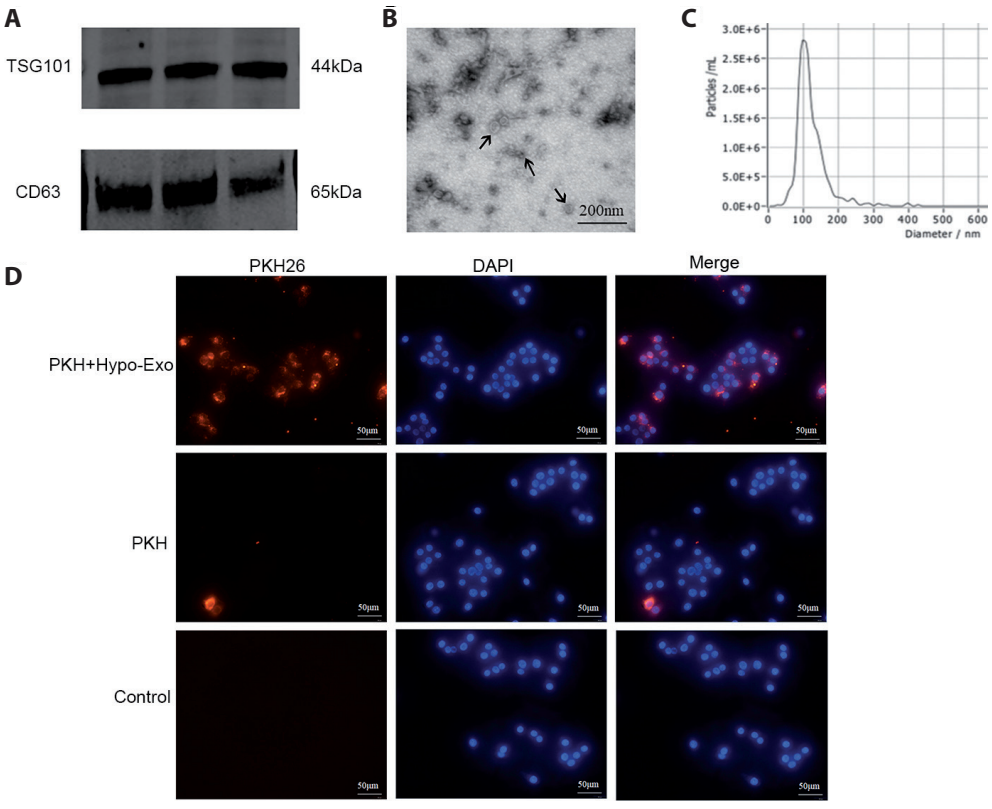

Figure 2. Characterization of exosomes derived from cardiomyocytes. **A.** The surface makers (TSG101 and CD63) of Hypo-Exo were detected by Western blotting. **B.** TEM detected morphological characterization of Hypo-Exo, and the representative exosomes were indicated with black arrows. Scale bar, 200 nm. **C.** The size distribution of Hypo-Exo was detected by NTA. **D.** Uptake of Hypo-Exo by macrophages *in vitro*. Hypo-Exo was engulfed by RAW264.7 cells *in vitro*. The Hypo-Exo was labeled with PKH26 (red fluorescence). Nuclei were counterstained with DAPI. Samples were imaged using a ZEISS LSM710. Scale bar, 50 μm.

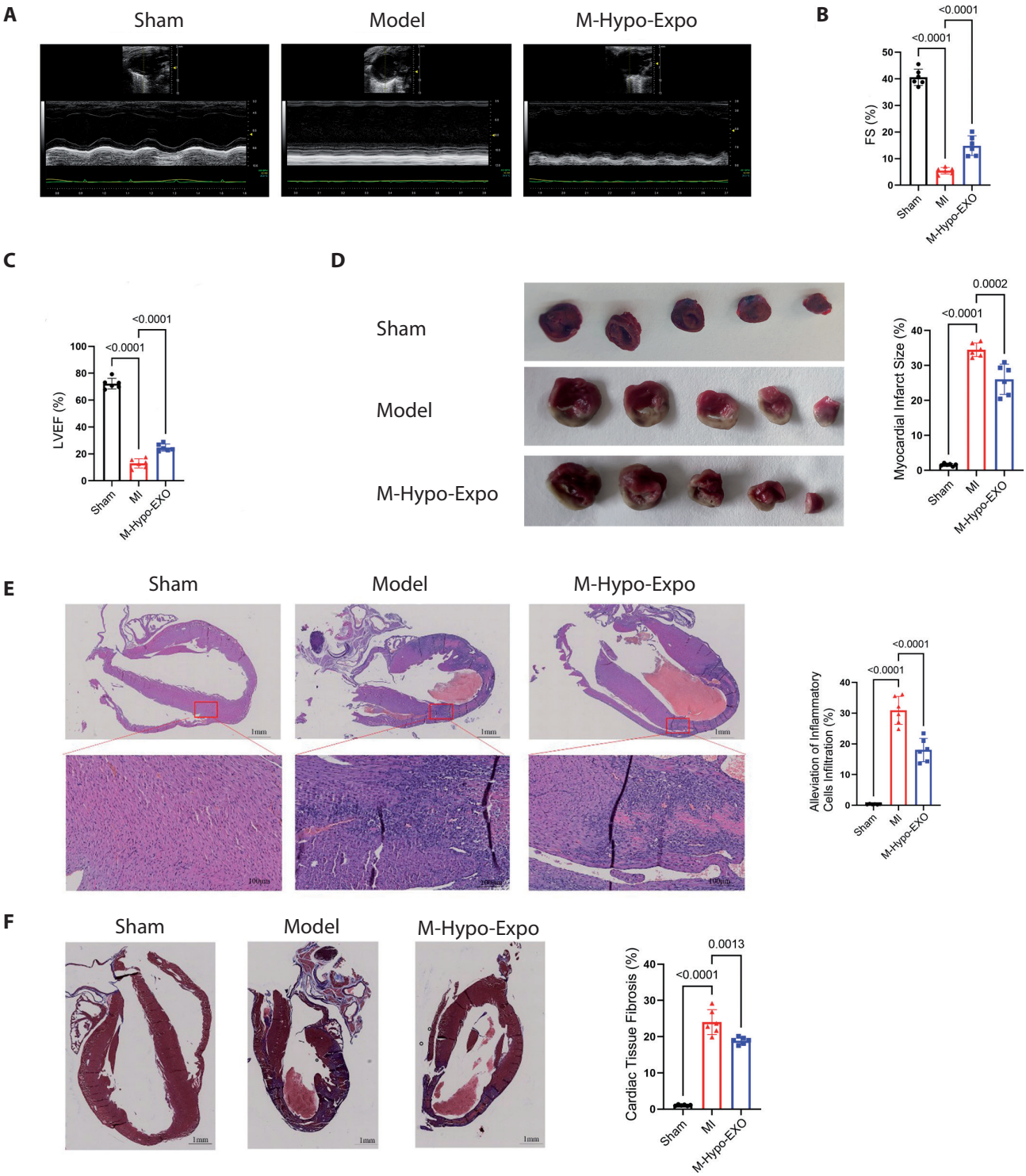

Figure 3. Effect of Hypo-Exo on the heart tissue in myocardial infarction mice. **A.** M-mode echocardiograms from mice of different groups ($n = 6$ each group). The expression level of fraction shortening (FS, **B**) and left ventricular ejection fraction (LVEF; **C**) ($n = 6$ each group). **D.** The infarct area was determined by TTC staining. The ischemic area showed pale and the viable myocardium showed red. Infarct area was quantified as INF/AAR×100%. **E.** Images of HE staining in the cardiac tissues. The scale bar of the above images is 1 mm, and the scale bar of the bellow images is 100 μm, 20× magnification. **F.** Images of Masson staining respectively. The myocardial collagenous fiber was stained blue, and the myocardial fiber was stained red. Scale bar, 1 mm. The alleviation of fibrosis was quantified by the ImageJ in the Masson staining. Sham, sham group; MI, myocardial infarction injury model group; MI+Hypo-Exo, MI + model exosomes group. (See online version for color figure.)

myocardial infarction in the MI group, compared with the sham group. Compared with the MI group, the infarct size decreased in the MI+Hypo-Exo group.

According to H&E staining, compared with the Sham group, gross structural changes were presented in the MI group, including a large number of inflammatory cells infiltration and necrosis in the myocardium of the heart. These pathological features of cardiac structure improved after Hypo-Exo treatment (Fig. 3E).

Masson staining was used to observe the degree of fibrosis in cardiac tissues. The myocardial collagenous fiber was stained blue, and the myocardial fiber was stained red. The fibrosis of cardiac tissues in the MI group displayed a disorder arrangement and large amounts of collagen deposition com-

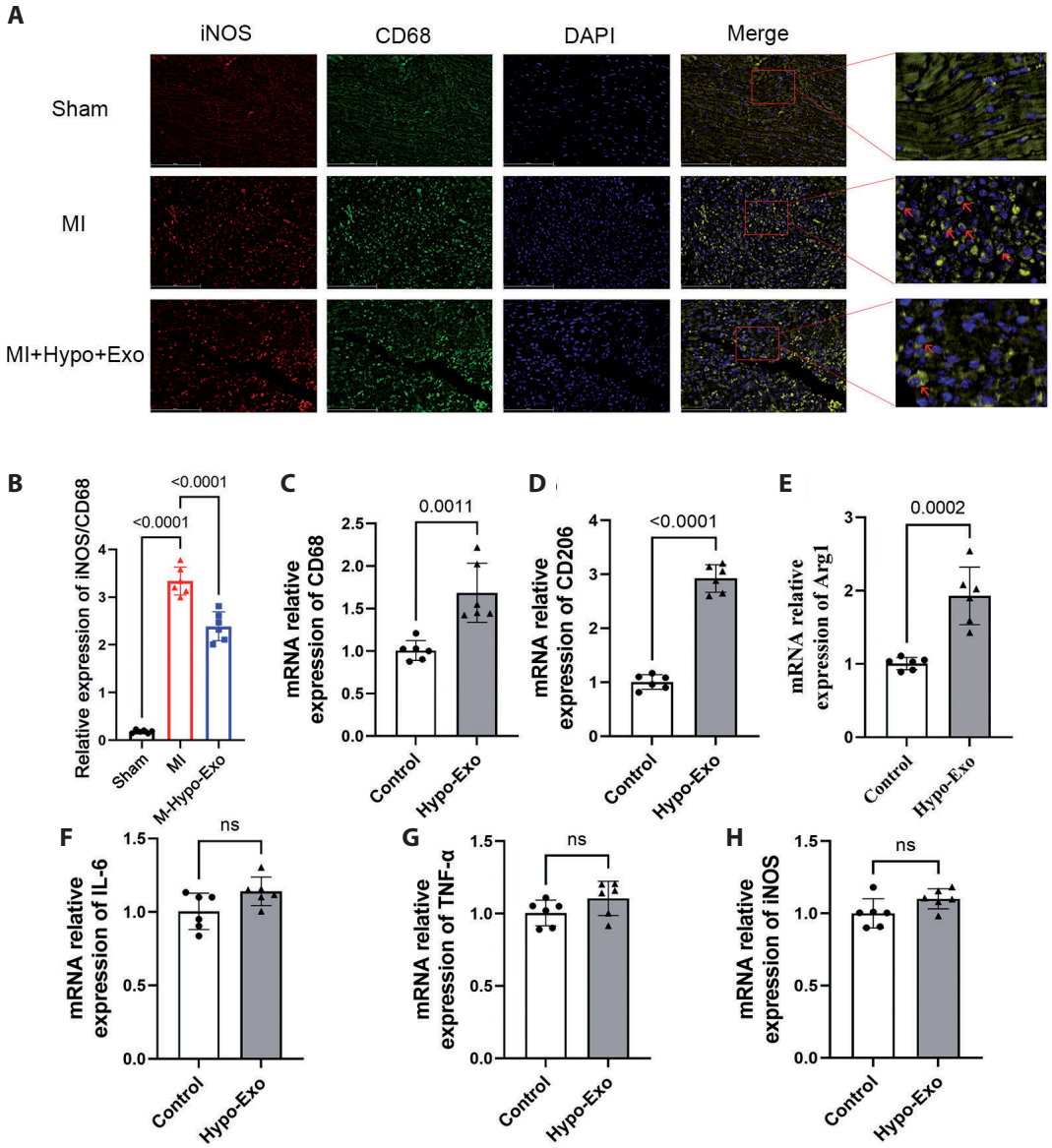

Figure 4. Effect of Hypo-Exo on macrophage polarization *in vitro* and *in vivo*. **A.** Images of immunofluorescence staining in the cardiac tissues, respectively. The heart slices were incubated at 4°C overnight with mixtures of two primary antibodies (anti-CD68 and anti-iNOS), followed by mixtures of secondary antibodies (Alexa Fluor 488-Labelled Donkey Anti-Rabbit IgG antibody and Alexa Fluor 555-Labelled Donkey Anti-Mouse IgG antibody). Nuclei were counterstained with DAPI. Samples were imaged using a ZEISS LSM710. The positive expression of iNOS/CD68 was indicated in MI and MI+Hypo-Exo groups with red arrows. Scale bar, 50μm. **B.** The relative intensity expression of iNOS/CD68 in Sham, MI, and MI-Hypo-Exo groups (n = 6 in each group). The mRNA expression levels of CD68 (**C**), CD206 (**D**), Arg1 (**E**), IL-6 (**F**), TNF-α (**G**), and iNOS (**H**) in RAW264.7 cells cocultured with Hypo-Exo, respectively (n = 6 in each group).

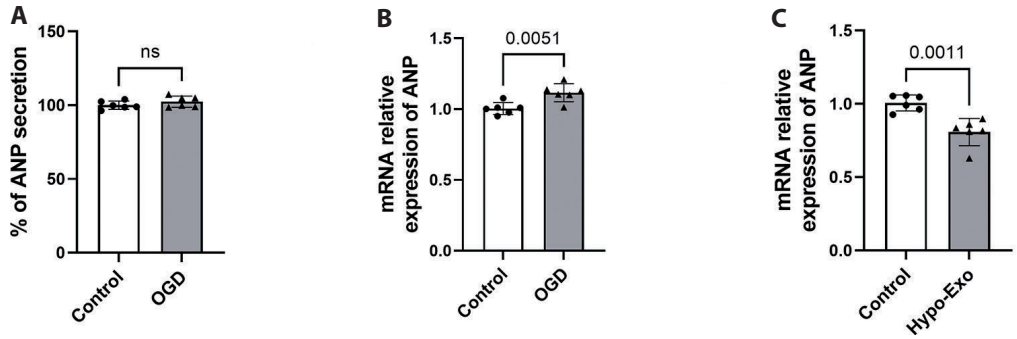

Figure 5. The ANP secretion in the supernatant of OGD and the mRNA expression levels of ANP in RAW264.7 cells. **A.** ELISA assays for the amount of ANP released in the supernatant of OGD ($n = 6$ in each group). RT-qPCR analysis for the expression of ANP in RAW264.7 cells cocultured with the supernatant of OGD (**B**) and Hypo-Exo (**C**) ($n = 6$ in each group).

pared with the sham group. Hypo-Exo treatment alleviated the effects of myocardial infarction on myocardial fibrosis (Fig. 3F).

Hypo-Exo could reduce macrophage polarization towards M1 subtype in vivo and increase macrophage polarization towards M2 subtype in vitro

Immunofluorescence staining was used to observe the macrophage polarization in cardiac tissues. The relative intensity expression of iNOS/CD68 was significantly increased in the MI group compared with the Sham group. However, the relative intensity expression of iNOS/CD68 was decreased in the MI+Hypo-Exo compared with the MI group. The results prompted that Hypo-Exo could reduce macrophage polarization towards M1 subtype (Fig. 4A,B).

To exploit the regulating effects of Hypo-Exo on macrophage polarization, we examined the change of macrophage marker expression of CD68, M1 (IL-6, TNF-α and iNOS) and M2 (CD206 and Arg1). The mRNA expression of macrophage biomarker CD68 (Fig. 4C), and M2 macrophage biomarkers CD206 and Arg1 (Fig. 4D,E) in the Hypo-Exo group were significantly increased compared with the control group. However, there was no difference in the mRNA levels of IL-6, TNF-α, and iNOS between the control and Hypo-Exo groups (Fig. 4F–H, F: $p = 0.0602 > 0.05$; G: $p = 0.1245 > 0.05$; H: $p = 0.0735 > 0.05$). These results demonstrated that Hypo-Exo could induce macrophages to exhibit the M2 subtype.

Hypo-Exo could inhibit the mRNA expression of ANP in RAW264.7 cells

ELISA analysis was used to measure the amount of ANP released in the supernatant of OGD in H9c2 cells, and there was no difference in the ANP secretion between the control and OGD groups (Fig. 5A, $p = 0.2449 > 0.05$).

As shown in Figure 5B, the mRNA expression of ANP in the supernatant-stimulated RAW264.7 cells was increased compared with the control group. However, as shown in Figure 5C, the mRNA expression of ANP in the Hypo-Exo-treated RAW264.7 cells decreased compared with the control group.

Hypo-Exo could promote the mRNA expression of NPR-A and microRNAs (miR-425, miR-155, and miR-1-3p) in vitro

ANP is a hormone/paracrine/autocrine factor regulating cardiovascular homeostasis by guanylyl cyclase natriuretic peptide receptor (NPR-A), and plays an important role also in regulating inflammatory and immune systems by altering macrophages functions and cytokines secretion (Mezzasoma et al. 2016). Furthermore, research has demonstrated that a mechanism of ANP production that would be related to some microRNAs, such as miR-425, miR-155 and miR-1-3p. The miRNAs could interact with the NPPA 3' UTR and regulate ANP levels (Wu et al. 2016). To exploit how Hypo-Exo influences the ANP mRNA expression, the expression of NPR-A, miR-425, miR-155 and miR-1-3p was detected by RT-qPCR. As shown in Figure 6, the expression of NPR-A, miR-425, miR-155, and miR-1-3p in the Hypo-Exo group was significantly increased compared with the control group.

The supernatant of OGD could induce macrophages to exhibit the M1 subtype in vitro

To observe the expression and macrophage polarization after myocardial infarction, we used the oxygen-glucose deprivation model to simulate myocardial infarction *in vitro.* We diluted the OGD supernatant of H9c2 at a ratio of 1:100 using complete DMEM medium. RT-qPCR was used to analyze the genetic levels of activation profiles. The

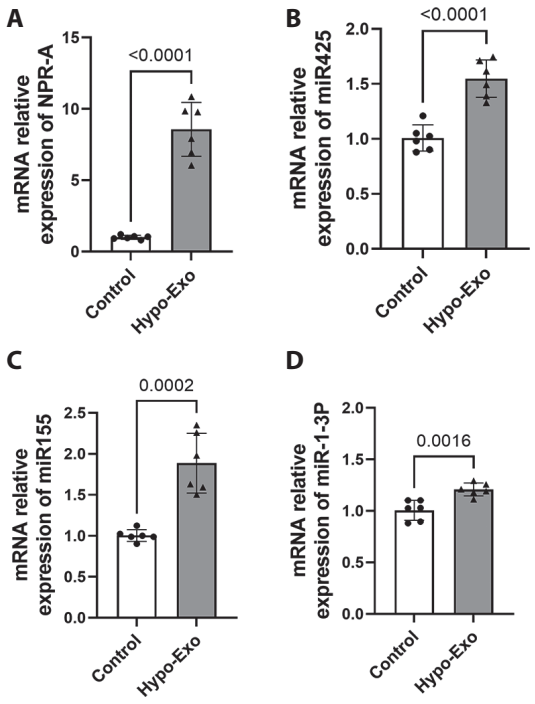

Figure 6. Effect of Hypo-Exo on the mRNA expression of NPR-A, miR-425, miR-155, and miR-1-3p in RAW264.7 cells. The mRNA expression levels of NPR-A (**A**), miR-425 (**B**), miR-155 (**C**) and miR-1-3p (**D**) in RAW264.7 cells cocultured with Hypo-Exo, respectively (n = 6 in each group).

mRNA expression of macrophage biomarker CD68 (Fig. 7A) in the OGD group was increased compared with the control group. The mRNA expression of M1 macrophage biomarkers iNOS, IL-6, and TNF-α (Fig. 7B–D) in the OGD group was significantly higher than that in the control group. These results demonstrated that the supernatant of OGD could induce macrophages to exhibit the M1 subtype.

Discussion

We applied the Hypo-Exo by myocardial injection for the model of mouse coronary ligation, and the Hypo-Exo showed significant cardiac protection in return. To investigate the M2 polarization mediated by Hypo-Exo, we observed that macrophages, upon phagocytosing the Hypo-Exo, exhibited inhibited expression of ANP, a crucial regulator in polarizing macrophages. Additionally, we observed upregulated expression of three miRNAs targeting the mRNA of ANP within the Hypo-Exo. Conversely, the supernatant derived from cardiomyocytes cultured under OGD, the source of Hypo-Exo, promoted M1 macrophage polarization, eliciting pro-inflammatory effects while simultaneously elevating ANP expression.

Increasing evidence highlights the therapeutic value of exosomes in cardiac repair after myocardial infarction, particularly those derived from stem cells (Sahoo and Losordo 2014; Zhao et al. 2019) and local inflammatory cells (Zhu et al. 2018; Liu et al. 2020; Zhang et al. 2022). Furthermore, different cell-derived exosomes play a crucial role in modulating the polarization of local macrophages, as supported by studies on their communication with macrophages. A recent study (Zhang et al. 2022) indicates that cardiomyocytes under hypoxia conditions secrets exosomes to induce RAW264.7 cells into M2 macrophages, providing protection against oxidative stress-induced injury. Consistent with previous studies indicating the innate ability of macrophages to engulf exosomes (Phinney et al. 2015; Hsieh et al. 2018), we observed in Figure 2 that $CD68^+$ macrophages primarily engulfed the Hypo-Exo *in vitro*. However, the M2 phenotypes induced by Hypo-Exo *in vitro* may not fully represent the anti-inflammatory effects of exosomes *in vivo*. Given the limitations of the amount and stability of exosomes in circulation, we employed myocardial injection as the delivery method in a mouse model of coronary ligation. The echocardiography and H&E staining results indicated that the direct myocardial injection of Hypo-Exo significantly improved cardiac functions and reduced the ischemic area (Fig. 3). These results suggest that the therapeutic effect of exosomes in myocardial ischemia is likely to be exerted through the

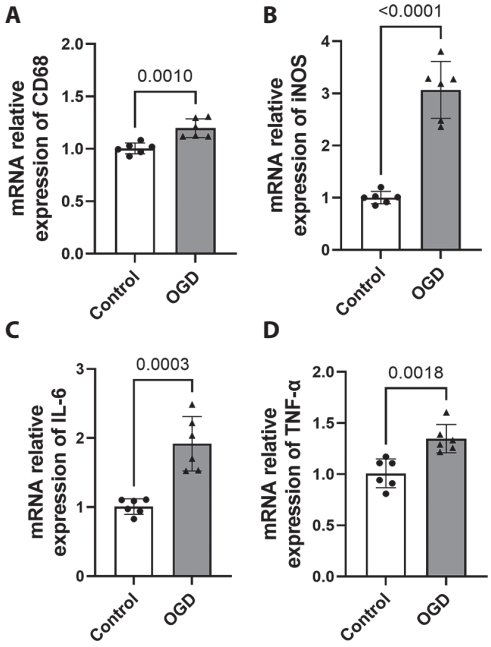

Figure 7. Effect of supernatant of OGD on macrophage polarization in RAW264.7 cells. The mRNA expression levels of CD68 (**A**), iNOS (**B**), IL-6 (**C**), and TNF-α (**D**) in RAW264.7 cells, respectively (n = 6 in each group).

uptake by local macrophages and the regulation of macrophage functional status.

Immunofluorescence staining of cardiac tissues showed that Hypo-Exo could reduce macrophage polarization towards M1 macrophages (Fig. 4A,B). To investigate the regulatory effects of Hypo-Exo on macrophage polarization, we treated RAW264.7 cells with Hypo-Exo and observed their activation and polarization towards M2 macrophages. This was evident from the upregulation of mRNA expression of CD68, CD206 and Arg1 (the markers of M2 macrophages), while the expression of markers associated with M1 macrophages, including IL-6, TNF-α, and iNOS, did not differ significantly compared to the control group. These findings suggest that the cardioprotective effects of cardiomyocyte-derived Hypo-Exo may rely on its potential to induce M2 macrophage polarization (Shiraishi et al. 2016) (Fig. 4). While macrophage plasticity presents a promising target for therapeutic development, the phenotypic profile of cardiac macrophages is complex and influenced by the surrounding tissue microenvironment. Apart from cytokines and chemokines, cardiomyocyte-derived ANP is upregulated and secreted in response to various pathophysiological stimuli. ANP administration has been shown to improve left ventricular function following global myocardial ischemia-reperfusion in hypoxic hearts (Fujii et al. 2012). Furthermore, direct evidence supports ANP's ability to deactivate the NF-kB/NALP3/caspase-1 signaling pathway through its binding to NPR-A, a macrophage surface receptor (Mezzasoma et al. 2016). In addition to its paracrine actions, ANP expression is significantly upregulated in LPS-activated murine macrophages (Vollmar and Schulz 1995). It acts as an autocrine regulator, maintaining immune response homeostasis by reducing iNOS at the transcriptional and post-transcriptional levels (Kiemer and Vollmar 1998). These results reinforce the anti-inflammatory and immunomodulatory effects of ANP.

In this study, we found that OGD-treated H9c2 cells did not increase the ANP products in the supernatants (Fig. 5A). Therefore, the M2 polarization may not be achieved through the hypoxia-induced ANP secretion by myocardial cells. Intriguingly, compared to an increased mRNA expression of ANP in the supernatant stimulation, we found that the ANP mRNA expression was downregulated in the Hypo-Exo-treated RAW264.7 cells (Fig. 5C). To exploit how Hypo-Exo influences the ANP mRNA expression, we screened three miRNAs that had been reported to target the ANP mRNA, including miR-425, miR-155, and miR-1-3p (Wu et al. 2016; Peet et al. 2020). All three miRNAs were upregulated in the Hypo-Exo-treated RAW264.7 cells (Fig. 6B–D), indicating that the miRNAs carried by Hypo-Exo degraded the ANP products. Notably, our findings indicate that Hypo-Exo significantly stimulated NPR-A mRNA expression (Fig. 6A), suggesting that it enhances the affinity between ANP and NPR-A, thereby augmenting its anti-inflammatory properties. After confirming Hypo-Exo as a communicator between macrophages and cardiomyocytes, we directly exposed RAW264.7 cells to the OGD-conditioned supernatant to observe the macrophage activation and polarization. Consistent with the results obtained using LPS-activated macrophages, OGD-conditioned supernatant upregulated the mRNA expression of ANP and induced M1 polarization in RAW264.7 cells, while increasing the mRNA expression level of pro-inflammation cytokines such as iNOS, IL-6, and TNF-α (Fig. 7). These results suggest that increased expression of ANP may be an intrinsic signaling pathway to regulate the cell polarization of macrophages, by which ANP plays crucial roles in participating in the homeostatic regulation of immune response. Since this experiment focuses more on the protective effect of Hypo-Exo on myocardial cells after myocardial infarction, the intrinsic relationship between the expression level of ANP and the polarization of macrophages was not explored in the experiment. The related mechanisms are worth further exploration.

In summary, we found that Hypo-Exo exerted an intrinsic modulator for cardiac repair after myocardial infarction, and surrounding M2 polarization induced by Hypo-Exo might be one of the pivotal mechanisms in the recovery process. Here we also demonstrate a novel mechanism where Hypo-Exo engulfed by surrounding macrophages carried miRNAs to degrade the ANP mRNA at post-transcription, indicating that the regulatory effect of ANP on macrophage activation may not be limited to ANP binding to the NPR-A receptor on macrophages.

Conclusions

Myocardial cell death under hypoxic conditions during myocardial infarction stimulates macrophage activation and triggers an inflammatory response. We found that Hypo-Exo, secreted by myocardial cells, played a positive role in protecting heart function after myocardial infarction. This effect is partly dependent on the polarization of macrophages to M2 after phagocytosis, which plays a role in local inflammation self-limitation. After creatively applying Hypo-Exo in the myocardial infarction mouse model through intramyocardial injection, we provide insights for developing novel therapeutics and delivering therapeutic cargo for ischemic heart diseases.

Statement of ethics. The animal experimental procedures and welfare followed the Ethics Review Committee for Animal Experimentation of New Drug Evaluation Center of Hebei Yiling Medical Research Institute (protocol number: N20221122).

Conflict of interests. All authors have no financial, personal, or other relationships with other people or organizations that could inappropriately influence the work. The authors declare that there is no conflict of interests.

Author contributions. MY-W, CZ and TT-L: methodology, writing-original draft preparation, data curation; TS and YY-H: methodology, data curation; WW-C and MG: methodology, data curation. YL and YL-H: conceptualization, writing- reviewing and editing.

Funding. This study was supported by the Natural Science Foundation of Hebei Province (H2019106059) and S&T Program of Hebei (NO. E2020100001).

Data availability statement. The data used to support the findings of this study are available from the corresponding author upon request.

References

Anderson JL, Morrow DA (2017): Acute myocardial infarction. N. Engl. J. Med. **376,** 2053-2064 https://doi.org/10.1056/NEJMra1606915

Benecke L, Coray M, Umbricht S, Chiang D, Figueiró F, Muller L (2021): Exosomes: Small EVs with large immunomodulatory effect in glioblastoma. Int. J. Mol. Sci. **22,** 3600 https://doi.org/10.3390/ijms22073600

Fu S, Ping P, Wang F, Luo L (2018): Synthesis, secretion, function, metabolism and application of natriuretic peptides in heart failure. J. Biol. Eng. **12,** 2 https://doi.org/10.1186/s13036-017-0093-0

Fujii Y, Ishino K, Tomii T, Kanamitsu H, Fujita Y, Mitsui H, Sano S (2012): Atrionatriuretic peptide improves left ventricular function after myocardial global ischemia-reperfusion in hypoxic hearts. Artif. Organs **36,** 379-386 https://doi.org/10.1111/j.1525-1594.2011.01358.x

Gao L, Wang L, Wei Y, Krishnamurthy P, Walcott GP, Menasche P, Zhang J (2020): Exosomes secreted by hiPSC-derived cardiac cells improve recovery from myocardial infarction in swine. Sci. Transl. Med. **12,** eaay1318 https://doi.org/10.1126/scitranslmed.aay1318

Hsieh CH, Tai SK, Yang MH (2018): Snail-overexpressing cancer cells promote M2-like polarization of tumor-associated macrophages by delivering MiR-21-abundant exosomes. Neoplasia **20,** 775-788 https://doi.org/10.1016/j.neo.2018.06.004

Jung K, Kim P, Leuschner F, Gorbatov R, Kim JK, Ueno T, Nahrendorf M, Yun SH (2013): Endoscopic time-lapse imaging of immune cells in infarcted mouse hearts. Circ. Res. **112,** 891-899 https://doi.org/10.1161/CIRCRESAHA.111.300484

Jung M, Ma Y, Iyer RP, DeLeon-Pennell KY, Yabluchanskiy A, Garrett MR, Lindsey ML (2017): IL-10 improves cardiac remodeling after myocardial infarction by stimulating M2 macrophage polarization and fibroblast activation. Basic Res. Cardiol. **112,** 33 https://doi.org/10.1007/s00395-017-0622-5

Kiemer AK, Vollmar AM (1998): Autocrine regulation of inducible nitric-oxide synthase in macrophages by atrial natriuretic peptide. J. Biol. Chem. **273,** 13444-13451 https://doi.org/10.1074/jbc.273.22.13444

Kiemer AK, Vollmar AM (2001): The atrial natriuretic peptide regulates the production of inflammatory mediators in macrophages. Ann. Rheum. Dis. **60,** iii68-70 https://doi.org/10.1136/ard.60.90003.iii68

Krylatov AV, Tsibulnikov SY, Mukhomedzyanov AV, Boshchenko AA, Goldberg VE, Jaggi AS, Erben RG, Maslov LN (2021): The role of natriuretic peptides in the regulation of cardiac tolerance to ischemia/reperfusion and postinfarction heart remodeling. J. Cardiovasc. Pharmacol. Ther. **26,** 131-148 https://doi.org/10.1177/1074248420952243

Lee WW, Marinelli B, van der Laan AM, Sena BF, Gorbatov R, Leuschner F, Dutta P, Iwamoto Y, Ueno T, Begieneman MP, et al. (2012): PET/MRI of inflammation in myocardial infarction. J. Am. Coll. Cardiol. **59,** 153-163 https://doi.org/10.1016/j.jacc.2011.08.066

Liu S, Chen J, Shi J, Zhou W, Wang L, Fang W, Zhong Y, Chen X, Chen Y, Sabri A, Liu S (2020): M1-like macrophage-derived exosomes suppress angiogenesis and exacerbate cardiac dysfunction in a myocardial infarction microenvironment. Basic Res. Cardiol. **115,** 22 https://doi.org/10.1007/s00395-020-0781-7

Ma Y, Mouton AJ, Lindsey ML (2018): Cardiac macrophage biology in the steady-state heart, the aging heart, and following myocardial infarction. Transl. Res. **191,** 15-28 https://doi.org/10.1016/j.trsl.2017.10.001

Malliaras K, Zhang Y, Seinfeld J, Galang G, Tseliou E, Cheng K, Sun B, Aminzadeh M, Marban E (2013): Cardiomyocyte proliferation and progenitor cell recruitment underlie therapeutic regeneration after myocardial infarction in the adult mouse heart. EMBO Mol. Med. **5,** 191-209 https://doi.org/10.1002/emmm.201201737

Mezzaroma E, Toldo S, Farkas D, Seropian IM, Van Tassell BW, Salloum FN, Kannan HR, Menna AC, Voelkel NF, Abbate A (2011): The inflammasome promotes adverse cardiac remodeling following acute myocardial infarction in the mouse. Proc. Natl. Acad. Sci. USA **108,** 19725-19730 https://doi.org/10.1073/pnas.1108586108

Mezzasoma L, Antognelli C, Talesa VN (2016): Atrial natriuretic peptide down-regulates LPS/ATP-mediated IL-1beta release by inhibiting NF-kB, NLRP3 inflammasome and caspase-1 activation in THP-1 cells. Immunol. Res. **64,** 303-312 https://doi.org/10.1007/s12026-015-8751-0

Moskalik A, Niderla-Bielinska J, Ratajska A (2022): Multiple roles of cardiac macrophages in heart homeostasis and failure. Heart Fail. Rev. **27,** 1413-1430 https://doi.org/10.1007/s10741-021-10156-z

Murray PJ, Allen JE, Biswas SK, Fisher EA, Gilroy DW, Goerdt S, Gordon S, Hamilton JA, Ivashkiv LB, Lawrence T, et al. (2014): Macrophage activation and polarization: nomenclature and experimental guidelines. Immunity **41,** 14-20 https://doi.org/10.1016/j.immuni.2014.06.008

Nichols M, Townsend N, Scarborough P, Rayner M (2014): Cardiovascular disease in Europe 2014: epidemiological update. Eur. Heart J. **35,** 2929

https://doi.org/10.1093/eurheartj/ehu299
Peet C, Ivetic A, Bromage DI, Shah AM (2020): Cardiac monocytes and macrophages after myocardial infarction. Cardiovasc. Res. **116,** 1101-1112
https://doi.org/10.1093/cvr/cvz336
Phinney DG, Di Giuseppe M, Njah J, Sala E, Shiva S, St Croix CM, Stolz DB, Watkins SC, Di YP, Leikauf GD, et al. (2015): Mesenchymal stem cells use extracellular vesicles to outsource mitophagy and shuttle microRNAs. Nat. Commun. **6,** 8472
https://doi.org/10.1038/ncomms9472
Sahoo S, Losordo DW (2014): Exosomes and cardiac repair after myocardial infarction. Circ. Res. **114,** 333-344
https://doi.org/10.1161/CIRCRESAHA.114.300639
Shapouri-Moghaddam A, Mohammadian S, Vazini H, Taghadosi M, Esmaeili SA, Mardani F, Seifi B, Mohammadi A, Afshari JT, Sahebkar A (2018): Macrophage plasticity, polarization, and function in health and disease. J. Cell Physiol. **233,** 6425-6440
https://doi.org/10.1002/jcp.26429
Shiraishi M, Shintani Y, Shintani Y, Ishida H, Saba R, Yamaguchi A, Adachi H, Yashiro K, Suzuki K (2016): Alternatively activated macrophages determine repair of the infarcted adult murine heart. J. Clin. Invest. **126,** 2151-2166
https://doi.org/10.1172/JCI85782
Sica A, Erreni M, Allavena P, Porta C (2015): Macrophage polarization in pathology. Cell Mol. Life Sci. **72,** 4111-4126
https://doi.org/10.1007/s00018-015-1995-y
Thery C, Amigorena S, Raposo G, Clayton A (2006): Isolation and characterization of exosomes from cell culture supernatants and biological fluids. Curr. Protoc. Cell Biol. **3,** 22
https://doi.org/10.1002/0471143030.cb0322s30
Vandergriff A, Huang K, Shen D, Hu D, Hensley MT, Caranasos TG, Qian L, Cheng K (2018): Targeting regenerative exosomes to myocardial infarction using cardiac homing peptide. Theranostics **8,** 1869-1878
https://doi.org/10.7150/thno.20524
Virag JA, Lust RM (2011): Coronary artery ligation and intramyocardial injection in a murine model of infarction. J. Vis. Exp. **52,** 2581
https://doi.org/10.3791/2581-v
Vollmar AM, Schulz R (1995): Expression and differential regulation of natriuretic peptides in mouse macrophages. J. Clin. Invest. **95,** 2442-2450
https://doi.org/10.1172/JCI117944
Wu C, Arora P, Agha O, Hurst LA, Allen K, Nathan DI, Hu D, Jiramongkolchai P, Smith JG, Melander O, et al. (2016): Novel MicroRNA regulators of atrial natriuretic peptide production. Mol. Cell Biol. **36,** 1977-1987
https://doi.org/10.1128/MCB.01114-15
Xiong YY, Gong ZT, Tang RJ, Yang YJ (2021): The pivotal roles of exosomes derived from endogenous immune cells and exogenous stem cells in myocardial repair after acute myocardial infarction. Theranostics **11,** 1046-1058
https://doi.org/10.7150/thno.53326
Zhang Z, Xu Y, Cao C, Wang B, Guo J, Qin Z, LuY, Zhang J, Zhang L, Wang J, et al. (2022): Exosomes as a messager to regulate the crosstalk between macrophages and cardiomyocytes under hypoxia conditions. J. Cell Mol. Med. **26,** 1486-1500
https://doi.org/10.1111/jcmm.17162
Zhao J, Li X, Hu J, Chen F, Qiao S, Sun X, Gao L, Xie J, Xu B (2019): Mesenchymal stromal cell-derived exosomes attenuate myocardial ischaemia-reperfusion injury through miR-182-regulated macrophage polarization. Cardiovasc. Res. **115,** 1205-1216
https://doi.org/10.1093/cvr/cvz040
Zhu LP, Tian T, Wang JY, He JN, Chen T, Pan M, Xu L, Zhang HX, Qiu XT, Li CC, et al. (2018): Hypoxia-elicited mesenchymal stem cell-derived exosomes facilitates cardiac repair through miR-125b-mediated prevention of cell death in myocardial infarction. Theranostics **8,** 6163-6177
https://doi.org/10.7150/thno.28021

Received: November 13, 2024
Final version accepted: April 16, 2025

doi: 10.4149/gpb_2025022

Supplementary Material

Hypoxia-conditioned cardiomyocyte-derived exosomes attenuate myocardial injury *via* ANP-mediated M2 macrophage polarization

Mingye Wang[1,*], Chi Zhao[2,*], Tongtong Li[1,3,*], Tao Song[4], Yuanyuan Hao[4], Wenwen Cui[4], Min Guan[5], Yunlong Hou[1,2,6,7] and Yang Li[5]

[1] *College of Integrated Traditional Chinese and Western Medicine, Hebei University of Chinese Medicine, Shijiazhuang, Hebei, China*
[2] *Hebei Medical University, Shijiazhuang, Hebei, China*
[3] *Affiliated Yiling Hospital of Hebei Medical University, Shijiazhuang, Hebei, China*
[4] *Shijiazhuang Yiling Pharmaceutical Co., Ltd, New Drug Evaluation Center, Shijiazhuang, Hebei, China*
[5] *Department of Cardiology, The Fourth Affiliated Hospital of Harbin Medical University, Nangang District, Harbin, Heilongjiang, China*
[6] *State Key Laboratory for Innovation and Transformation of Luobing Theory, Shijiazhuang, Hebei, China*
[7] *Shijiazhuang New Drug Technology Innovation Center of Compound Traditional Chinese Medicine, Shijiazhuang, Hebei, China*

Supplementary Table

Table S1. Experimental animal allocation and sample sizes

Analysis		Group			Notes
		Sham	MI	MI+Hypo-Exo	
Total animals *per* group		12	12	12	Randomly divided into two subgroups
Subgroup 1: TTC staining		6	6	6	Infarct size quantification
Subgroup 2: Echocardiography		6	6	6	Assessment before animals were sacrificed
Histopathology	HE staining	6	6	6	Animal sacrificed and the hearts collected. The same hearts used for: Morphological assessment, Fibrosis quantification, and Protein expression analysis
	Masson staining	6	6	6	
	Immuno-fluorescence	6	6	6	

Subgroup 1 (n = 6/group): dedicated to TTC staining. Subgroup 2 (n = 6/group): echocardiographic assessments were conducted in all animals before the surgical procedure. Hearts from these animals were sectioned, and serial sections were used for HE staining, Masson staining, and immunofluorescence analyses.